Article

Immunity

Expansion and Activation of CD103+ Dendritic Cell Progenitors at the Tumor Site Enhances Tumor Responses to Therapeutic PD-L1 and BRAF Inhibition

Graphical Abstract

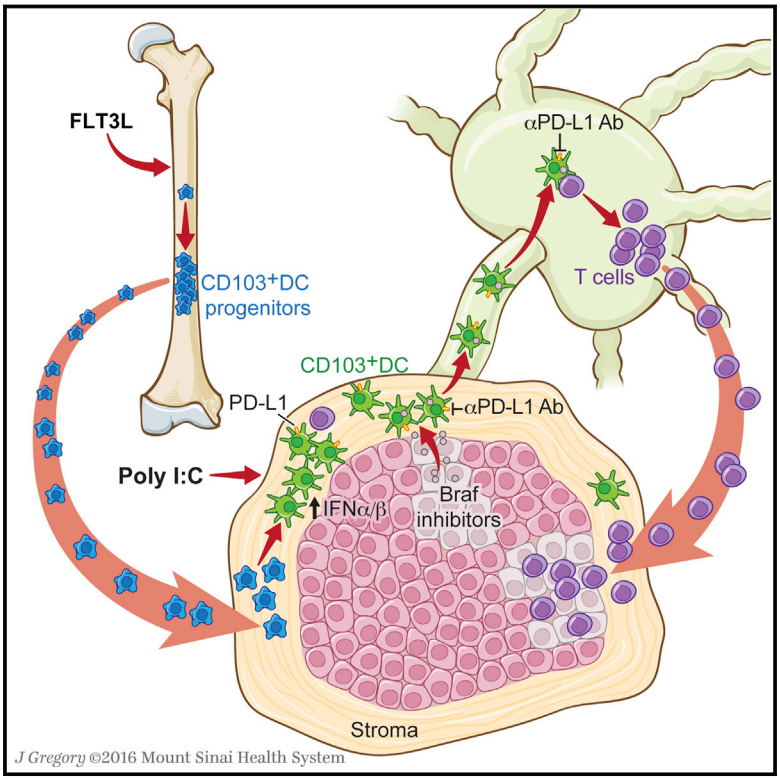

Authors

Hélène Salmon, Juliana Idoyaga, Adeeb Rahman, ..., Joshua Brody, Florent Ginhoux, Miriam Merad

Correspondence

miriam.merad@mssm.edu

In Brief

Large numbers of melanoma patients develop resistance to targeted therapy or fail to respond to checkpoint inhibition. Merad and colleagues show that FLT3L and poly I:C combined treatment, which expands and activates CD103+ DC progenitors at the tumor site, enhances tumor responses to BRAF and PD-L1 blockade.

Highlights

- CD103+ DCs are uniquely able to transport intact antigens to the TdLN and prime CD8+ T cells
- CD103+ DCs are required to induce anti-PD-L1-Ab-mediated anti-tumor immunity
- Combined FLT3L and poly I:C therapy induces expansion and activation of CD103+ DC progenitors in tumors
- Combined FLT3L and poly I:C therapy enhances tumor responses to BRAF and checkpoint blockade

Salmon et al., 2016, Immunity *44*, 924–938
April 19, 2016
http://dx.doi.org/10.1016/j.immuni.2016.03.012

CellPress

CellPress

Immunity
Article

Expansion and Activation of CD103$^+$ Dendritic Cell Progenitors at the Tumor Site Enhances Tumor Responses to Therapeutic PD-L1 and BRAF Inhibition

Hélène Salmon,[1,2,3] Juliana Idoyaga,[5] Adeeb Rahman,[4] Marylène Leboeuf,[1,2,3] Romain Remark,[2,3] Stefan Jordan,[1,2,3] Maria Casanova-Acebes,[1,2,3] Makhzuna Khudoynazarova,[1,2,3] Judith Agudo,[2,3,4] Navpreet Tung,[1,2,3] Svetoslav Chakarov,[9] Christina Rivera,[1,2,3] Brandon Hogstad,[1,2,3] Marcus Bosenberg,[6] Daigo Hashimoto,[7] Sacha Gnjatic,[2,3] Nina Bhardwaj,[2,3] Anna Karolina Palucka,[8] Brian D. Brown,[2,3,4] Joshua Brody,[2,3] Florent Ginhoux,[9] and Miriam Merad[1,2,3,*]

[1]Department of Oncological Sciences
[2]Tisch Cancer Institute
[3]Immunology Institute
[4]Department of Genetics and Genomic Sciences
Icahn School of Medicine at Mount Sinai, New York, NY 10029, USA
[5]Department of Microbiology and Immunology, Stanford University School of Medicine, Stanford, CA 94305, USA
[6]Yale University School of Medicine, New Haven, CT 06510, USA
[7]Department of Hematology, Hokkaido University Graduate School of Medicine, Sapporo 060-8638, Japan
[8]The Jackson Laboratory for Genomic Medicine, Farmington, CT 06032, USA
[9]Singapore Immunology Network, Agency for Science, Technology and Research, Biopolis 138648, Singapore
*Correspondence: miriam.merad@mssm.edu
http://dx.doi.org/10.1016/j.immuni.2016.03.012

SUMMARY

Large numbers of melanoma lesions develop resistance to targeted inhibition of mutant BRAF or fail to respond to checkpoint blockade. We explored whether modulation of intratumoral antigen-presenting cells (APCs) could increase responses to these therapies. Using mouse melanoma models, we found that CD103$^+$ dendritic cells (DCs) were the only APCs transporting intact antigens to the lymph nodes and priming tumor-specific CD8$^+$ T cells. CD103$^+$ DCs were required to promote anti-tumoral effects upon blockade of the checkpoint ligand PD-L1; however, PD-L1 inhibition only led to partial responses. Systemic administration of the growth factor FLT3L followed by intratumoral poly I:C injections expanded and activated CD103$^+$ DC progenitors in the tumor, enhancing responses to BRAF and PD-L1 blockade and protecting mice from tumor rechallenge. Thus, the paucity of activated CD103$^+$ DCs in tumors limits checkpoint-blockade efficacy and combined FLT3L and poly I:C therapy can enhance tumor responses to checkpoint and BRAF blockade.

INTRODUCTION

Two classes of drugs, inhibitors of BRAF signaling (Flaherty et al., 2010) and checkpoint inhibitors (Sharma and Allison, 2015a and 2015b), have recently achieved substantial survival advantages in melanoma patients. Despite initial high clinical responses to BRAF blockade in BRAF^{V600E}-mutated melanoma patients, most tumor lesions relapse within a few months after therapy initiation (Flaherty et al., 2010). BRAF inhibition can induce tumor cell death and the release of tumor antigens and therefore represents a unique opportunity to increase T cell immunity against readily available tumor-associated antigens (Kroemer et al., 2013).

Three checkpoint inhibitors have been actively explored clinically, including antibodies (Abs) to cytotoxic lymphocyte antigen 4 (CTLA-4), programmed cell death 1 (PD-1), and the checkpoint ligand PD-L1 (Page et al., 2014). PD-L1 is expressed mostly on steady-state antigen-presenting cells (APCs) and can be upregulated upon exposure to inflammatory signals (Keir et al., 2008) on APCs and tumor cells. Upon T cell receptor (TCR) engagement with cognate antigens, PD-L1 binds to PD-1 on T cells and modulates T cell activation by inducing TCR stop signals (Fife et al., 2009; Yokosuka et al., 2012).

Despite significant clinical benefits, high numbers of cancer patients fail to respond to checkpoint blockade. Prior studies suggest that checkpoint inhibition might not be sufficient in patients who have limited tumor immune cell infiltration (Fuertes et al., 2011; Gajewski et al., 2013; Herbst et al., 2014; Sharma and Allison, 2015a). However, although T cells are found accumulating in the tissue stroma surrounding the tumor mass in most human tumors, they are rarely found interacting with tumor cells (Galon et al., 2006; Salmon et al., 2012). In a fraction of patients who resist anti-PD-L1 monoclonal Ab (mAb) therapy, CD8$^+$ T cells localize at the edge of the tumors, whereas they accumulate in the tumor mass in patients who respond to PD-L1 blockade (Herbst et al., 2014; Tumeh et al., 2014), suggesting that, in addition to PD-L1 inhibition, strategies aimed at promoting T cell accumulation in the tumor mass are essential for the induction of therapeutic immunity.

Through their ability to produce T-cell-specific chemokines and present antigens together with costimulatory or inhibitory

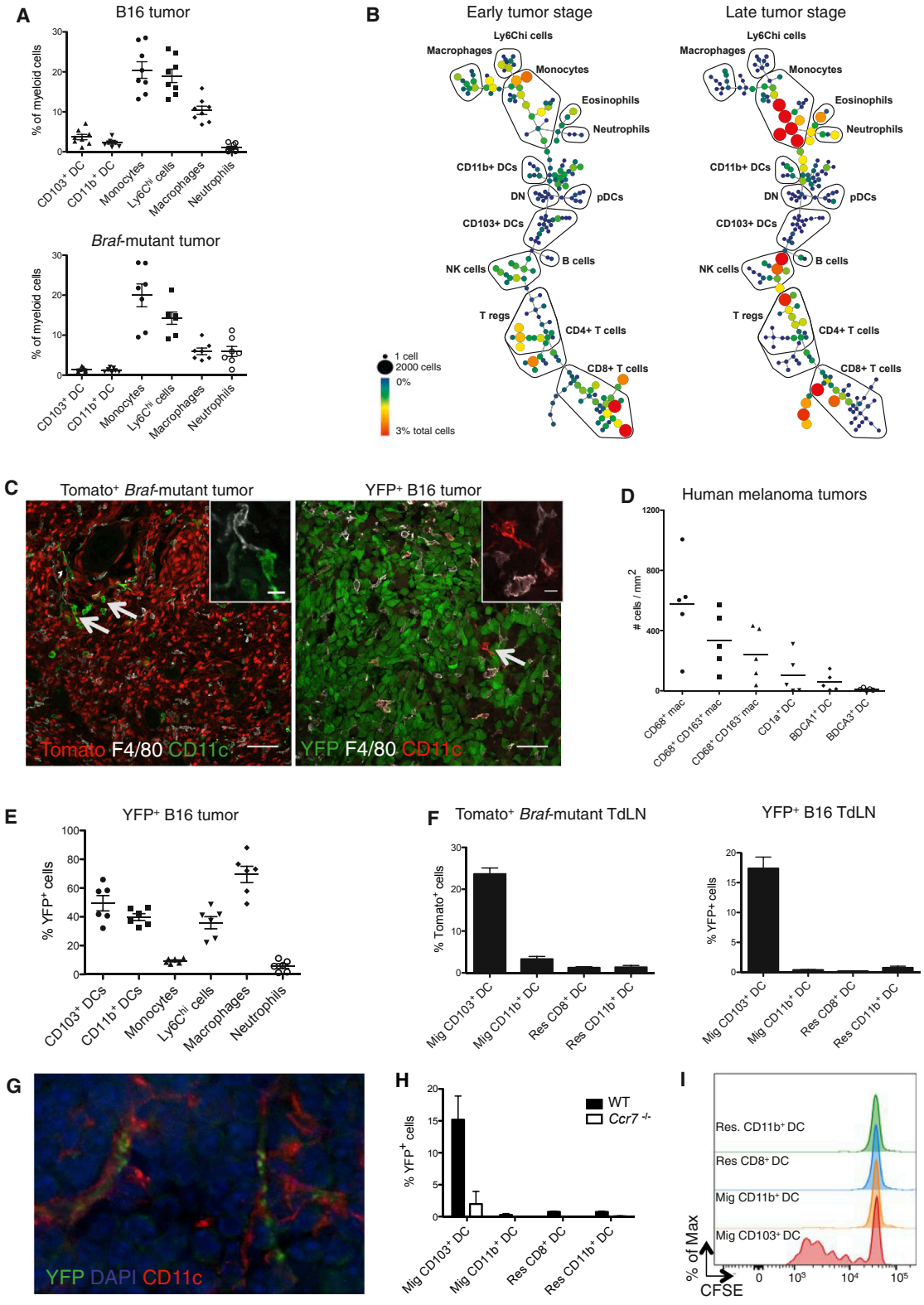

Figure 1. CD103+ DCs Are Uniquely Able to Transport Intact Antigens to the TdLN

B16 and *Braf*-mutant tumors and LNs were analyzed at day 15 and 25, respectively, unless specified otherwise.

(A) Frequency of each myeloid cell population among total myeloid cells infiltrating B16 (n = 8) and *Braf*-mutant tumors (n = 7). See Figure S1A for gating strategy. Shown is the mean ± SEM of 2 or 3 independent experiments.

(legend continued on next page)

signals, tumor-associated APCs are best poised to shape anti-tumoral effector immunity. Most inflamed tissues harbor heterogeneous populations of APCs that comprise dendritic cells (DCs), macrophages, monocytes, and monocyte-derived cells (Merad et al., 2013). Tissue-resident DCs consist of two functionally specialized subsets: the $CD103^+$-$CD8^+$ DCs, which excel in the priming and cross-presentation of cell-associated antigens to $CD8^+$ T cells, and $CD11b^+$ DCs, which are more potent at driving $CD4^+$ helper T cell responses (Merad et al., 2013). Analogous counterparts to these populations have been identified in humans and include $CD141^+$ and $CD1c^+$ DCs, respectively (Guilliams et al., 2014). Previous results suggest that melanoma lesions enriched in type I interferon (IFN)-induced genes are also rich in T cells and that type I IFN production by the $CD103^+$-$CD8^+$ DC lineage controls spontaneous T cell priming to tumor antigens (Fuertes et al., 2011). Thus, the composition of the tumor-associated myeloid compartment most likely plays a key role in tumor response to checkpoint blockade.

In this study, we examined the composition of tumor-associated myeloid cells of two different melanoma lesions at different time points during tumor growth. We probed their contribution to the transport of tumor antigens to the tumor-draining lymph node (TdLN), to induction of anti-tumoral effector T cells, and to shaping clinical response to checkpoint inhibition. Our results revealed that increased myeloid cell commitment to the $CD103^+$ DC lineage and activation of intratumoral $CD103^+$ DCs could substantially enhance the clinical response to checkpoint and BRAF blockade.

RESULTS

$CD103^+$ and $CD11b^+$ DCs Represent Minor Cell Populations Infiltrating *Braf*-Mutant and B16 Melanoma Lesions

To characterize the diversity of tumor-associated myeloid cells, we used two experimental models of melanoma tumors: B16 tumor graft and the *Tyr*::*CreER*;$Braf^{CA}$*Pten*^{loxP}*Ctnnb1*^{loxex3} tumor model in which the $Braf^{V600E}$ mutation, *Pten* deletion, and a mutated form of β-catenin that increases its stability are enforced in melanocytes upon cutaneous application of 4-hydroxytamoxifen (4-HT), leading to the formation of advanced melanoma lesions within 3 weeks (Damsky et al., 2011).

In both tumor lesions, myeloid cells accounted for more than 60% of $CD45^+$ cells and consisted mostly of monocytes and macrophages. DCs represented only a minor cell population, reaching no more than 5% of myeloid cells (Figure 1A). To more thoroughly evaluate the tumor-infiltrating immune populations, we used time-of-flight mass cytometry (CyTOF) and analyzed B16 tumors at two different time points. SPADE analysis revealed an accumulation of monocytes that paralleled a reduced DC to monocyte-derived cell ratio over time (Figure 1B). Similar data were obtained via flow cytometry (Figure S1B). Both $CD103^+$ and $CD11b^+$ DC subsets were present in tumor lesions, although in very low numbers, along with macrophages and $Ly6C^{hi}MHCII^{hi}$ cells, referred to as monocyte-derived cells. Monocyte-derived cells and macrophages expressed the monocyte markers CCR2 and CD115, the macrophage markers MertK, F4/80, and CD64, as well as detectable levels of CD11c (Figure S1C).

To characterize DC and macrophage localization in the tumor mass, we generated fluorescent-reporter inducible melanoma lesions by crossing C57BL/6 *Tyr*::*CreER*;$Braf^{CA}$*Pten*^{loxP} mice with Tomato reporter mice. We also used B16-YFP tumor cell lines in which melanoma cells are positive for the yellow fluorescent protein (YFP). Whereas macrophages and monocyte-derived cells were distributed throughout the tumor, DCs were sparsely distributed and rarely infiltrated the tumor mass (Figure 1C). Consistent with these findings, human melanoma lesions were poorly infiltrated by DCs, in particular $CD1c^+$ and $CD141^+$ DCs, in comparison to $CD68^+$ macrophages, which accumulated throughout the tumor (Figure 1D and S1D). These results emphasize the paucity of tumor-infiltrating DCs in mouse and human melanoma lesions.

$CD103^+$ DCs Are the Only Intratumoral Myeloid Cell Population that Transports Intact Antigens to the TdLNs

We tracked the capture of tumor-associated fluorescent antigens by each myeloid cell compartment by using confocal microscopy and flow cytometry (Figures 1E–1H). Macrophages were by far the most potent cells at capturing tumor-associated fluorescence (Figures 1E and S1E), which accumulated as puncta in intracellular compartments, consistent with antigen phagocytosis (Figure S1F). Although most myeloid cells captured tumor-associated fluorescence at the tumor site, $CD103^+$ DCs were the only myeloid cells carrying intact Tomato

(B) CyTOF analysis of tumor-infiltrating immune cells at early (day 10) and late (day 16) stages of B16 tumor growth. Gated live $CD45^+$ cells were clustered via SPADE and based on 27 markers. Trees are representative of two experiments with similar results.
(C) Representative confocal images showing $CD11c^+$ $F4/80^-$ DCs and macrophages and monocyte-derived $CD11c^{+/-}$ $F4/80^+$ cells and $CD11c^+$ $F4/80^-$ DCs in $Tomato^+$ *Braf*-mutant and B16-YFP tumors; scale bar, 50 μm. The right upper corners show magnification of a DC and a macrophage or monocyte-derived cell; scale bar, 10 μm. Arrows show rare tumor-infiltrating DCs.
(D) Density of macrophages and DCs infiltrating human melanoma primary tumors (n = 5) quantified from tumor sections stained via multiplexed immunohistochemistry (Figure S1D).
(E) Frequency of YFP^+ cells infiltrating B16-YFP tumors. Shown is the mean ± SEM of two independent experiments (n = 6).
(F) Frequency of $Tomato^+$ and YFP^+ cells in skin migratory ($CD11c^+MHCII^{hi}$) and LN-resident ($CD11c^{hi}MHCII^+$) DCs in the LN-draining $Tomato^+$ *Braf*-mutant (left panel, n = 9) and B16-YFP tumors (right panel, n = 12). Shown is the mean ± SEM of four independent experiments.
(G) Representative image of a $CD11c^+$ cell harboring YFP^+ vesicles in the LN-draining B16-YFP tumors.
(H) Frequency of YFP^+ cells among migratory DCs isolated from the LN-draining B16-YFP tumors in WT or $Ccr7^{-/-}$ mice (n = 2). Shown is the mean ± SEM of one experiment (n=2).
(I) Migratory and LN-resident DCs were sorted from the LN-draining B16-OVA tumors and co-cultured with CFSE-labeled OT-I T cells (DC-T ratio = 1/3). Three days later, the proliferation of OT-I T cells was determined by CFSE dilution. Histograms represent one of two independent experiments with similar results.
See also Figure S1.

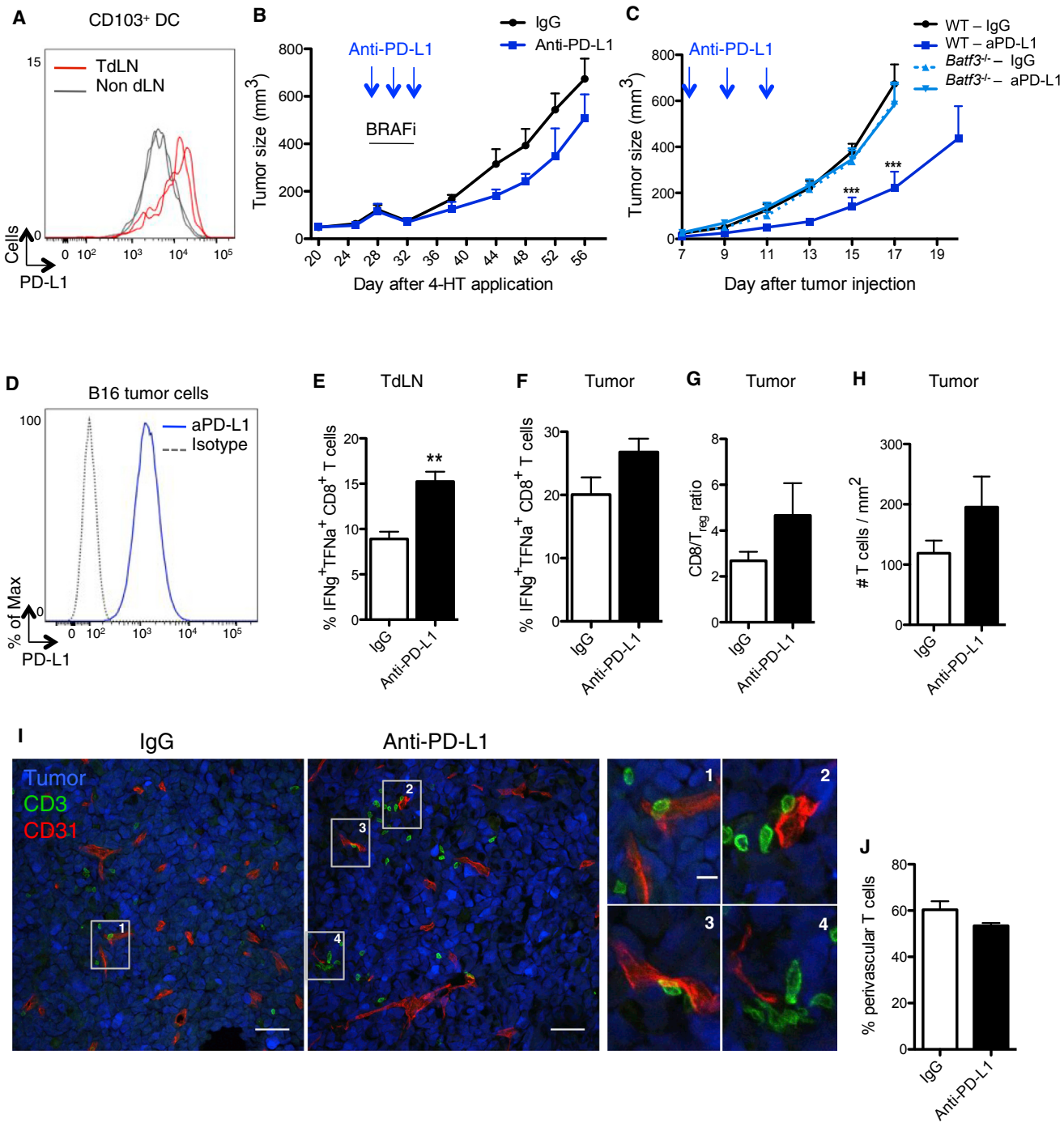

Figure 2. CD103⁺ DCs Control Tumor Response to PD-L1 Blockade

(A) PD-L1 expression on CD103⁺ DCs purified from B16 TdLNs (red lines) and non-draining LNs (gray lines), day 15 after tumor challenge. Representative flow cytometry histogram of two experiments.

(B) *Braf*-mutant mice were treated i.p. with either anti-PD-L1 or a control mAb on days 28 (tumor size: 100–150 μm^3), 30, and 32 after 4-HT topical application. All mice were treated with BRAF inhibitors from day 28 to 32. Shown is mean ± SEM of two independent experiments (n = 5 or 6).

(C) B16-tumor-bearing WT or *Batf3*$^{-/-}$ mice were treated i.p. with either anti-PD-L1 or a control mAb on days 7, 9, and 11 after tumor challenge. Tumor growth was followed for 17–20 days. Shown is the mean ± SEM of two independent experiments (n = 5–8).

(D) PD-L1 expression on cultured B16 tumor cells.

(E–J) Mice were inoculated with B16 tumor cells and treated as in (C).

(E and F) On day 15, mice were sacrificed, and CD8⁺ T cells from a TdLN (E) or tumor (F) were analyzed for the production of IFN-γ and TNF-α after 3 hr stimulation with PMA and ionomycin. Shown is the mean ± SEM of two independent experiments (n = 4 or 5 mice).

(legend continued on next page)

fluorescent proteins or YFPs to the TdLN, in both models (Figures 1F and 1G). YFP$^+$ CD103$^+$ DCs were strongly reduced in the TdLNs of mice lacking CCR7, a chemokine receptor required for DC migration to the LN (Förster et al., 1999), in comparison to *Ccr7*$^{+/+}$ mice, suggesting that tumor-associated fluorescence was actively transported by tissue-migratory CD103$^+$ DCs to the LN (Figure 1H). CD11b$^+$ migratory DCs, LN CD64$^+$ macrophages, and monocyte-derived cells were negative for Tomato and YFP (data not shown), suggesting that they either failed to transport tumor-associated antigens or efficiently degraded the fluorescence in the TdLN. To address this question, mice were injected with B16 tumors expressing the model antigen ovalbumin (B16-OVA), and migratory and LN-resident DCs were isolated from the TdLN by fluorescence-activated cell sorting (FACS) and co-cultured with OVA-specific TCR-transgenic OT-I CD8$^+$ T cells labeled with the cell proliferation dye, CFSE. Migratory CD103$^+$ DCs were the only cells able to promote OT-I T cell activation and proliferation (Figure 1I). Altogether, these results demonstrate the unique ability of tumor-infiltrating CD103$^+$ DCs to transport and cross-present tumor-associated antigens to CD8$^+$ T cells in the TdLN, leading to the differentiation of tumor-specific CD8$^+$ T cells.

CD103$^+$ DCs Are Required to Promote Anti-PD-L1-Ab-Mediated Anti-tumor Immunity

CD103$^+$ DCs expressed PD-L1 at high levels in the TdLN, in comparison to skin-migratory CD103$^+$ DCs present in the non-TdLN (Figure 2A), prompting us to examine whether PD-L1 blockade increases CD103$^+$ DC ability to prime CD8$^+$ T cells in the TdLN and tumor and promotes anti-tumor immunity.

Consistent with prior results (Spranger et al., 2014), PD-L1 blockade given alone or in combination with BRAF inhibition delayed B16 tumor growth (Figures 2B and 2C). To investigate the contribution of CD103$^+$ DCs to the anti-PD-L1 Ab effect, we compared B16 tumor growth upon PD-L1 blockade in wild-type (WT) or *Batf3*$^{-/-}$ mice, which lack CD103$^+$-CD8$^+$ DCs (Figure 2C). Despite the high expression of PD-L1 on B16 tumor cells (Figure 2D), the moderate but significant anti-tumoral effect mediated by PD-L1 blockade was lost in *Batf3*$^{-/-}$ mice. These results established that CD103$^+$ DCs controlled PD-L1-mediated anti-tumor immunity.

PD-L1 Blockade Fails to Significantly Promote CD8$^+$ T Cell Accumulation in the Tumor Mass

When combined with BRAF inhibitors, PD-L1 blockade delayed tumor growth but failed to prevent tumor relapse after interruption of BRAF inhibition (Figure 2B). Whereas PD-L2 expression increased on tumor migratory CD103$^+$ DCs, its expression was strongly reduced upon BRAF inhibition (Figure S2A), suggesting that the poor tumor response to PD-L1 and BRAF inhibitors was not due to upregulation of PD-L2.

Failure to respond to PD-L1 blockade has been shown to correlate with reduced expression of PD-L1 on tumor-infiltrating immune cells or the absence of CD8$^+$ T cell in the tumor mass prior to treatment (Herbst et al., 2014; Tumeh et al., 2014). Although PD-L1 inhibition increased the number of CD8$^+$ T cells producing IFN-γ and tumor-necrosis factor (TNF)-α in the TdLN (Figure 2E), the number of IFN-γ^+ TNF-α^+ CD8$^+$ T cells and the CD8$^+$ T cell to regulatory T cell (Treg) ratio did not significantly increase in anti-PD-L1-treated tumors (Figures 2F and 2G). Using tetramers, we quantified antigen presentation in the tumor and LN and observed a slight increase in the priming of tumor-specific CD8$^+$ T cells in both sites (Figure S2B). However, we also found that the tumor-infiltrating T cells remained mostly outside the tumor mass, accumulating mainly within the perivascular areas in the B16 model (Figures 2H–2J). This suggested that defects of T cell recruitment to the tumor site might contribute to the subdued response to anti-PD-L1 Ab. These data contrast with previously published results showing increased accumulation of intratumoral CD8$^+$ cells in Braf^{CA}Pten^{loxP} tumors treated with BRAF and PD-L1 blockade in comparison to BRAF blockade alone (Cooper et al., 2014). It is plausible that the additional β-catenin mutation present in our tumor model could have contributed to the limited T cell accumulation in the tumor. This would be consistent with recently published data showing that β-catenin expression in melanoma lesions alters chemokine production, thereby compromising DC and T cell recruitment (Spranger et al., 2015).

FLT3L Injections Dramatically Expand CD103$^+$ DC Progenitors in the Bone Marrow and Promote Their Accumulation and Proliferation in the Tumor Mass

We hypothesized that the paucity of CD103$^+$ DCs at the tumor site restricted the expansion of tumor-specific CD8$^+$ T cells and therefore limited anti-PD-L1 Ab anti-tumor efficacy. Another possibility was that the excess of highly phagocytic macrophages competed for antigen availability at the tumor site thereby limiting the ability of CD103$^+$ DCs to prime and activate CD8$^+$ T cells.

To expand CD103$^+$ DCs, we injected mice with the growth factor FMS-like tyrosine kinase 3 ligand (FLT3L, referred to hereafter as FL), a cytokine promoting hematopoietic progenitor commitment to the DC lineage as well as DC survival and proliferation in tissues (Liu and Nussenzweig, 2010). We found that nine daily injections of FL dramatically expanded CD103$^+$ DCs, which became the predominant myeloid cell population at the tumor

(G) CD8$^+$ T cell to Treg cell ratio 15 days after tumor challenge is shown as the mean ± SEM of two independent experiments (n = 4 or 5).
(H) B16-YFP tumors were harvested on day 13 (2 days after the last injection of anti-PD-L1 or control mAb) and stained with anti-CD3 mAb. The density of CD3$^+$ T cells infiltrating B16-YFP tumors was automatically quantified with Cell Profiler software from confocal images. Shown is the mean ± SEM of three independent experiments (n = 4–6; 12–16 tiled 20× images were analyzed per animal.)
(I) B16-YFP tumors (blue) were harvested and frozen on day 13 and stained for T cells (CD3$^+$; green) and blood vessels (CD31$^+$; red). Panels show confocal images (scale bar, 50 μm) representative of three experiments with similar results. Right panels show higher magnifications of T cells surrounding vessels (scale bar, 10 μm).
(J) As in (I), but the percentages of CD3$^+$ T cells found in perivascular areas ($\leq$30 μm from a CD31$^+$ vessel) were quantified with Cell Profiler software. Shown is the mean ± SEM of three independent experiments (n = 4–6).
See also Figure S2.

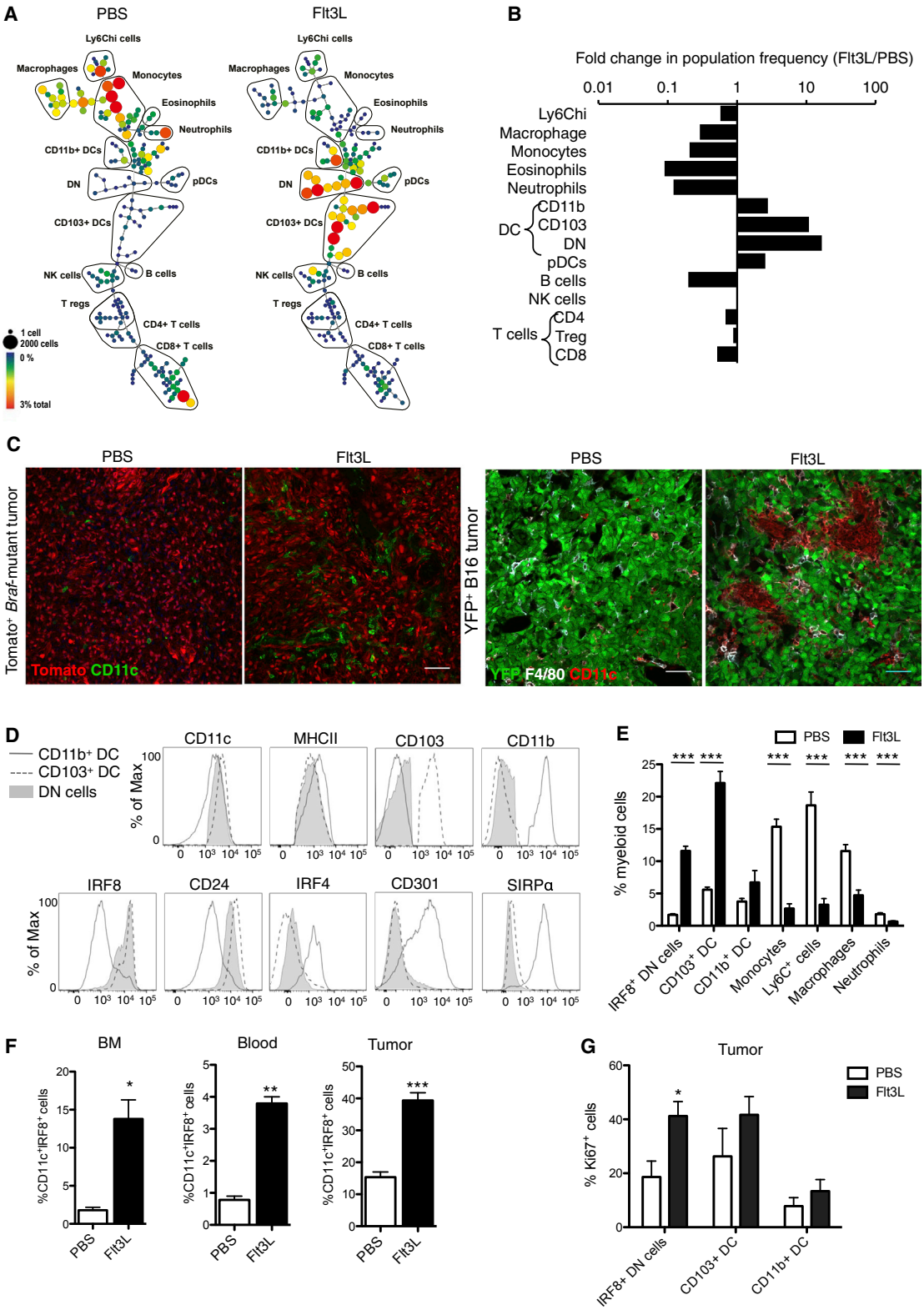

Figure 3. FL Injections Dramatically Expand CD103$^+$ DC Progenitors in the Bone Marrow and Promote Their Accumulation and Expansion in the Tumor Mass

(A) CyTOF analysis of tumor-infiltrating immune cells on day 13 after B16 tumor challenge in mice treated i.p. for 9 consecutive days starting at day 3 after tumor injection with 30 μg FL or PBS. SPADE trees were colored by relative population frequency out of total live CD45$^+$ cells. Five mice were pooled to build each SPADE tree. Trees are representative of two experiments with similar results.

(legend continued on next page)

site (Figures 3A–3C and 3E). To probe the origin of this dramatic DC expansion in the tumor, we analyzed the FL-induced changes in the bone marrow. We noted an expansion of MHCII^{hi}CD11c^{+}CD103^{-}CD11b^{-} cells lacking lineage markers (referred to as double negative [DN] cells) in the bone marrow, blood circulation, and tumor (Figures 3A, 3E, and 3F). More than 80% of the DN MHCII^{+}CD11c^{+} cells were positive for IRF8 (Figure 3D), a transcription factor required for the differentiation of CD103^{+} DCs but not CD11b^{+} DCs (Ginhoux et al., 2009) and lacked IRF4, the transcription factor required for the differentiation of CD11b^{+} DCs (Murphy et al., 2013) (Figure 3D). IRF8^{+} DN cells proliferated actively in the tumor (Figure 3G), suggesting that FL injections led to the expansion of DC progenitors committed to the CD103^{+} DC lineage and their accumulation at the tumor site. To directly address whether IRF8^{+} DN cells gave rise to CD103^{+} DCs, we sorted the DN cells from B16 tumors of FL-treated mice and cultured them in vitro in the presence of FL ± granulocyte-macrophage colony-stimulating factor (GM-CSF) as previously described (Sathe et al., 2011; Schlitzer et al., 2015) (Figure S3A). In FL-supplemented cultures, DN cells gradually differentiated into CD103^{+}CD11b^{-} DCs, whereas CD11b^{+} DCs remained unchanged. GM-CSF addition to the cultures further increased DN cell differentiation into CD103^{+} DCs but failed to promote the differentiation of CD11b^{+} DCs. This established that the mobilized IRF8^{+} DN cells were precursors for CD103^{+} DCs, consistent with the immature CD103^{+} DCs found in vivo in FL-treated tumors (Figure 4A). Altogether, these data suggest that FL administration led to the predominant expansion of CD103^{+} DC progenitors and immature CD103^{+} DCs at the tumor site.

FL and poly I:C Combined Therapy Significantly Enhances the Recruitment and Activation of Effector Anti-tumoral CD8^{+} T Cells in Melanoma Lesions

Immature DCs cannot efficiently prime T cells, and therefore we needed to promote the maturation of local FL-mobilized CD103^{+} DCs. Among APCs, CD103^{+} DCs and their human counterpart CD141^{+} DCs uniquely express Toll-like receptor 3 (TLR3) (Hashimoto et al., 2011). TLR3 recognizes viral double-stranded RNA and its synthetic analog polyriboinosinic:polyribocytidylic acid (poly I:C, referred to hereafter as pIC) and induces type I IFN production as well as DC maturation via the adaptor protein TIR-domain-containing adaptor-inducing IFN-β (TRIF) (Bogunovic et al., 2011; Bogunovic et al., 2009; Longhi et al., 2009; Matsumoto and Seya, 2008). Production of type I IFN by the CD103^{+}-CD8^{+} DC lineage is required for T cell priming against tumor antigens (Bogunovic et al., 2009; Fuertes et al., 2011). Thus, we chose intratumoral pIC delivery to activate CD103^{+} DCs, increase type I IFN availability at the tumor site, and limit potential immune adverse events due to CD103^{+} DC activation in other tissues (Figure S4A).

pIC injections upregulated the expression levels of the costimulatory molecules CD40, CD86, and MHCII on tumor-infiltrating CD103^{+} DCs (Figure 4A) and to a lesser extent on CD11b^{+} DCs (data not shown), indicating proper DC maturation and activation. The significant increase of DC progenitor and mature DC numbers in the tumor mass was accompanied by a significant increase of OVA-specific IFN-γ^{+} CD8^{+} OT-I cell frequencies in the TdLNs of mice injected with B16-OVA tumors and with OT-I cells, in comparison to control groups (Figure 4B). Combined FL-pIC also led to the expansion of CD8^{+} T cells specific to the melanocyte antigen gp100 in the TdLNs of B16-tumor-bearing mice (Figure 4C), suggesting that the combined therapy could also promote the priming and/or expansion of T cells specific for endogenous tumor-associated antigens. Although, in comparison to PBS injections, pIC injections led to reduced B16 tumor lesions, FL-pIC significantly enhanced tumor regression in comparison to tumors treated with PBS, FL alone, or pIC alone (Figure 4D).

Similar to what we observed with B16 tumors, FL-pIC treatment also significantly reduced *Braf*-mutant tumor growth in comparison to the PBS- and FL-treated groups (Figure 4E). Although not statistically significant, there was a clear trend toward a superior clinical effect in the FL-pIC-treated group compared to the pIC-treated mice.

We compared the anti-tumor effect of systemic versus intratumoral injections of pIC and observed, in a dose-equivalent manner, a much stronger anti-tumor effect when pIC was administered intratumorally (Figure 4F). Thus, intratumoral injections helped lower the pIC dose and reduce its potential toxicity.

Because a majority of patients who initially respond to BRAF blockade do relapse (Flaherty et al., 2010), we investigated whether FL-pIC combined treatment increases anti-tumor immunity to melanoma antigens released upon BRAF inhibition therapy and therefore prolongs tumor response to BRAF blockade in mice bearing *Braf*-mutant melanoma lesions (Figure S4B). Similarly to what was observed in B16-tumor-bearing mice, FL-pIC combined therapy enhanced the proliferation of gp100-specific T cells in the TdLN (Figure 4G) and significantly

(B) Fold changes in relative frequency of immune cell populations (identified by SPADE clustering performed in A) between FL- and PBS-treated mice.
(C) Representative confocal images of DCs infiltrating Tomato^{+} *Braf*-mutant tumors (red) and B16-YFP tumors (green) treated with 9 daily injections of FL or PBS starting on day 18 after 4-HT topical application (*Braf* mutant) or 3 days after tumor challenge (B16). Tumor biopsies were isolated and frozen 30 days (*Braf* mutant) and 15 days (B16) after tumor challenge. In *Braf*-mutant tumors, DCs were identified as CD11c^{+} cells (green), whereas in B16- tumors, DCs were identified as F4/80^{-}CD11c^{+} (red). Scale bar, 50 μm.
(D) Mice were treated as in A. Histograms show the expression of cell surface markers or transcription factors in CD103^{+} DCs (dashed line), CD11b^{+} DCs (gray line) and MHCII^{hi}CD11c^{+}Ly6C^{-}CD64^{-}CD103^{-}CD11b^{-} DN cells (full gray) infiltrating B16 tumors on day 13 after tumor challenge. Results shown are representative histograms of two experiments.
(E) Frequency of myeloid cell populations infiltrating B16 tumors in mice treated with FL or PBS as in (A). Results shown are the mean ± SEM of three independent experiments with a total of 8 mice.
(F) Frequency of MHCII^{hi}CD11c^{+}Ly6C^{-}CD64^{-}CD103^{-}CD11b^{-}IRF8^{+} (IRF8^{+} DN) cells in bone marrow, blood, and tumors of B16-tumor-bearing mice analyzed 2 days after nine daily injections of FL or PBS. Shown is the mean ± SEM of one experiment (n = 5).
(G) Frequency of Ki67^{+} cells among IRF8^{+} DN cells, CD103^{+} DCs, and CD11b^{+} DCs infiltrating B16-tumor sites analyzed 2 days after nine daily injections of FL or PBS. Shown is the mean ± SEM of two independent experiments (n = 4).
See also Figure S3.

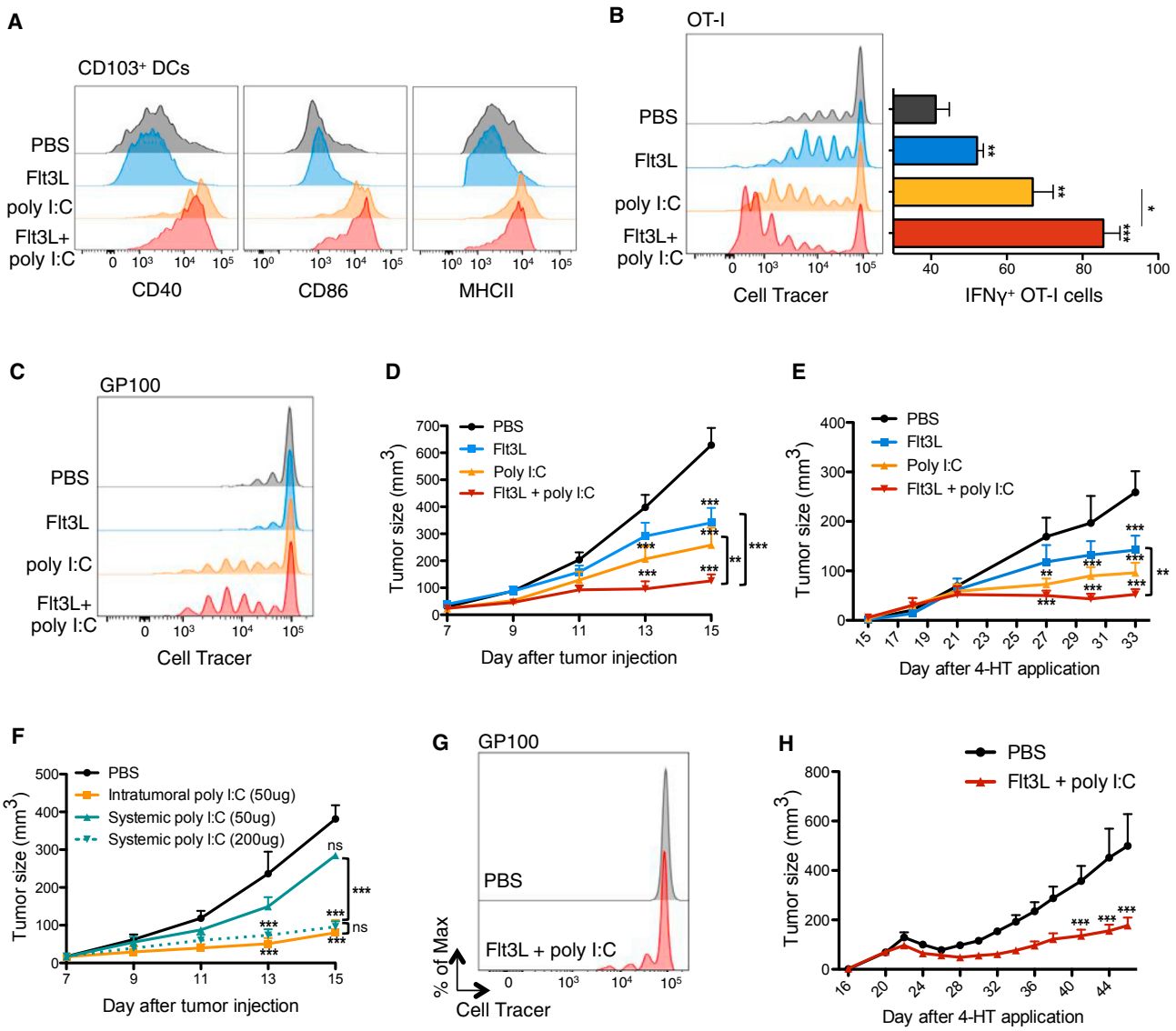

Figure 4. Combination of FL and In Situ TLR3 Ligand Promotes the Regression of B16 and *Braf*-Mutant Lesions

(A) Expression of CD40, CD86, and MHCII on tumor-infiltrating CD103$^+$ DCs upon treatment with i.p. FL and/or pIC or PBS as a control (treatment scheme in Figure S4A). Shown are representative histograms of two independent experiments.

(B) B16-OVA-bearing mice were treated with FL and pIC as in (A). At day 11, mice were adoptively transferred with violet-labeled OT-I T cells, 2 hr after the last injection of pIC or PBS. TdLN were harvested 3 days after OT-I T cell transfer and proliferation was assessed based on violet dilution via flow cytometry. Left panels show a representative histogram showing violet cell dilution in gated transferred OT-I T cell. Bar graph (right panel) shows the mean ± SEM. IFN-γ production by gated OT-I cells after in vitro re-stimulation with ovalbumin$_{257–264}$ peptide for 4 hr.

(C) B16-tumor-bearing mice were treated with FL and pIC as in (A) and adoptively transferred with violet-labeled gp100-specific T cells. TdLNs were harvested 4 days after i.v. injection of gp100-specific T cells, and their proliferation was assessed based on violet dilution via flow cytometry. Shown is a representative histogram of two independent experiments.

(D) B16-tumor-bearing mice were treated with FL, pIC, FL-pIC, or PBS as shown in (A). Graph shows the mean tumor growth ± SEM of four independent experiments (n = 7–12).

(E) *Braf*-mutant tumor-bearing mice were treated as in (A), with FL injections starting on day 15 after 4-HT application. Graphs show the mean tumor growth ± SEM of two independent experiments (n = 5).

(F) B16-tumor-bearing mice were treated with PBS (control) or pIC (50 μg or 200 μg) intratumorally or i.p. as in (A) (injections on days 7 and 11). Graph shows the mean tumor growth ± SEM of two independent experiments (n = 3–6 mice).

(G) *Braf*-mutant-tumor-bearing mice were treated as described in Figure S4B. On day 26, 2 hr after the last injection of FL-pIC or PBS, mice were adoptively transferred with violet-labeled gp100-specific T cells. TdLNs were harvested 4 days after gp100-specific T cell transferred cells and proliferation was assessed through Violet-Cell trace dilution. Shown is a representative histogram of two independent experiments.

(H) *Braf*-mutant-tumor-bearing mice were treated as described in Figure S4B. Graph shows the mean tumor growth ± SEM of two independent experiments (n = 5 or 6 mice).

See also Figure S4.

reduced tumor relapse after interruption of BRAF inhibitors in comparison to the control group (Figure 4H).

Therapeutic Immunity Induced by FL-pIC Combined Treatment Requires CD103$^+$ DCs and type I IFN

Although a slight T cell accumulation was induced upon BRAF inhibition alone, BRAF inhibition combined with FL-pIC treatment promoted a massive T cell infiltration throughout the tumor (Figures 5A and 5B). Accordingly, whereas T lymphocytes were almost absent in untreated B16 tumors, FL-pIC increased T cell frequency per mm in the tumor and promoted T cell proliferation in situ (Figures 5C–5E). FL-pIC treatment significantly increased the number of tumor-infiltrating antigen-specific cytolytic and IFN-γ^+ TNF-α^+ CD8$^+$ T cells (Figures 5F and 5G and S4C) and increased CD8$^+$ T cell to Treg cell ratio at the tumor site (Figure 5H).

Upon injections of the sphingosine 1 phosphate (S1P) receptor antagonist FTY-720, we found a drastic reduction in OT-I cell numbers in the tumors of FL-pIC-treated mice (Figures 5I and S5C). FTY-720 is known to prevent T cell egress from the LN (Figure S5D); therefore, these results could suggest that T cell priming in the TdLN is required to promote the FL-pIC anti-tumor response. Additional experiments will be required to further characterize the contribution of the TdLN versus the tumor site to the induction of anti-tumor immunity.

We then asked whether CD103$^+$ DCs controlled the FL-pIC-mediated anti-tumor effect. B16 tumors injected in *Batf3*$^{-/-}$ animals, which lack CD103$^+$ and CD8$^+$ DCs, did not respond to FL-pIC combined therapy (Figure 5J). Accordingly, effector T cells failed to accumulate in FL-pIC-treated tumors in *Batf3*$^{-/-}$ animals in comparison to WT animals (Figure 5K). These results strongly suggest that induction of anti-tumoral effector immunity in FL-pIC-treated mice is dependent on CD103$^+$ DCs.

Depletion of natural killer (NK) cells in FL-pIC-treated mice did not compromise tumor outcome (Figure 5L), indicating that NK cells were dispensable for the FL-pIC-mediated anti-tumor effect. In contrast, depletion of CD4$^+$ and CD8$^+$ T cells prior to FL-pIC injection reduced the FL-pIC therapeutic effect without totally abrogating it (Figure 5L), suggesting that the regression of primary tumors was partially dependent on T cell responses but also on innate immunity induced by CD103$^+$ DCs.

We found that B16 tumors injected into mice lacking the IFN alpha receptor (*Ifnar*$^{-/-}$) failed to respond to FL-pIC therapy (Figure S5A), which was consistent with prior studies showing that type I IFN signature at the tumor site correlates with anti-tumoral immunity (Fuertes et al., 2011). We found that, similarly to what occurred in *Ifnar*$^{-/-}$ mice, B16 tumors injected into *Ifnar*$^{-/-}$ bone marrow chimeric animals did not respond to FL-pIC treatment (Figure S5B).

pIC acts through two RNA sensors, TLR3 and melanoma differentiated antigen 5 (MDA5) (Kawai and Akira, 2010). TLR3, which is highly expressed on CD103$^+$ DCs but is lacking on other APCs (Miller et al., 2012), uses TRIF for the induction of type I IFN (Kawai and Akira, 2010). We reconstituted mice with bone marrow cells lacking TRIF so that immune cells were unable to respond to TLR3 signaling but should still be able to respond to MDA5. We found that the absence of TLR3-TRIF in immune cells greatly compromised the B16 tumor response to FL-pIC treatment (Figure S5B).

Altogether, these data suggest that CD103$^+$ DCs, as well as IFN alpha receptor and TRIF expression in the immune compartment, controlled the FL-pIC anti-tumoral effect.

FL and pIC Synergize with anti-PD-L1 Ab Treatment to Enhance Anti-tumor Responses to BRAF Inhibition

In accordance with previous studies, we found that in situ pIC injections substantially increased the expression of PD-L1 on intratumoral CD103$^+$ DCs (Figure 6A), suggesting that PD-L1 upregulation on APCs might limit the therapeutic efficacy of FL-pIC therapy. Thus, we compared the clinical outcome of mice treated with the combined FL-pIC and anti-PD-L1 Ab therapy (referred to as "tritherapy") to mice treated with FL-pIC or anti-PD-L1 Ab alone. The tritherapy dramatically increased the regression of B16 established tumors (Figure 6B). Accordingly, PD-L1 inhibition combined with FL-pIC further increased the number of IFN-γ^+ TNF-α^+ CD8$^+$ T cells in B16 TdLNs and tumors and increased the CD8$^+$ T cell to Treg cell ratio in tumors in comparison to mice treated with FL-pIC or anti-PD-L1 Ab alone (Figures 6C–6E). Treg cells' absolute numbers were not decreased, but their frequency was reduced due to increased recruitment and proliferation of CD8$^+$ T effector cells (data not shown).

The improved clinical outcome of B16 tumors treated with the tritherapy prompted us to test whether it could be used to further reduce the relapse of *Braf*-mutant lesions after interruption of BRAF inhibition. Whereas tumor growth was delayed but not abrogated in control groups treated with anti-PD-L1 Ab or FL-pIC alone, *Braf*-mutant lesions treated with the tritherapy were strongly reduced upon interruption of BRAF blockade (Figure 6F).

We then probed the tritherapy effect on secondary tumors that developed upon tumor rechallenge induced through 4-HT re-administration. Given that the secondary tumors did not receive any treatment, their regression should depend on a memory anti-tumor immune response induced upon treatment of the primary tumors. Thus, mice harboring *Braf*-mutant tumors were treated with the tritherapy, anti-PD-L1 Ab alone, or immunoglobulin G (IgG)-PBS, in addition to BRAF inhibition, as in Figure 6F. Ten days after treatment interruption, mice were rechallenged with 4-HT on the opposite flank of the treated primary tumors and analyzed one month later (Figure S6A). Compared to mice initially treated with anti-PD-L1 alone or with isotype control, mice in which the primary tumors were treated with the tritherapy developed much smaller secondary tumors accompanied with increased accumulation of IFN-γ^+ TNF-α^+ CD8$^+$ T cells in the TdLN along with massive T cell accumulation in the tumors (Figures 6G–6J). PD-L1 inhibition alone did not confer superior protective immunity compared to that of non-treated animals (Figures 6G–6J).

Tyr::*CreER*;*Braf*^{CA}*Pten*^{loxP}*Ctnnb1*^{loxex3} transgenic mice develop serial skin tumors on ears, eyes, paws, and tail within 2 months after primary tumor induction with 4-HT. These secondary tumors could represent either skin metastases or tumors that form due to leakiness of the cre-transgene. Consistent with our findings upon tumor rechallenge, mice in which the primary tumors were treated with the tritherapy in addition to BRAF inhibition had significantly reduced skin tumors (Figure 6K) in

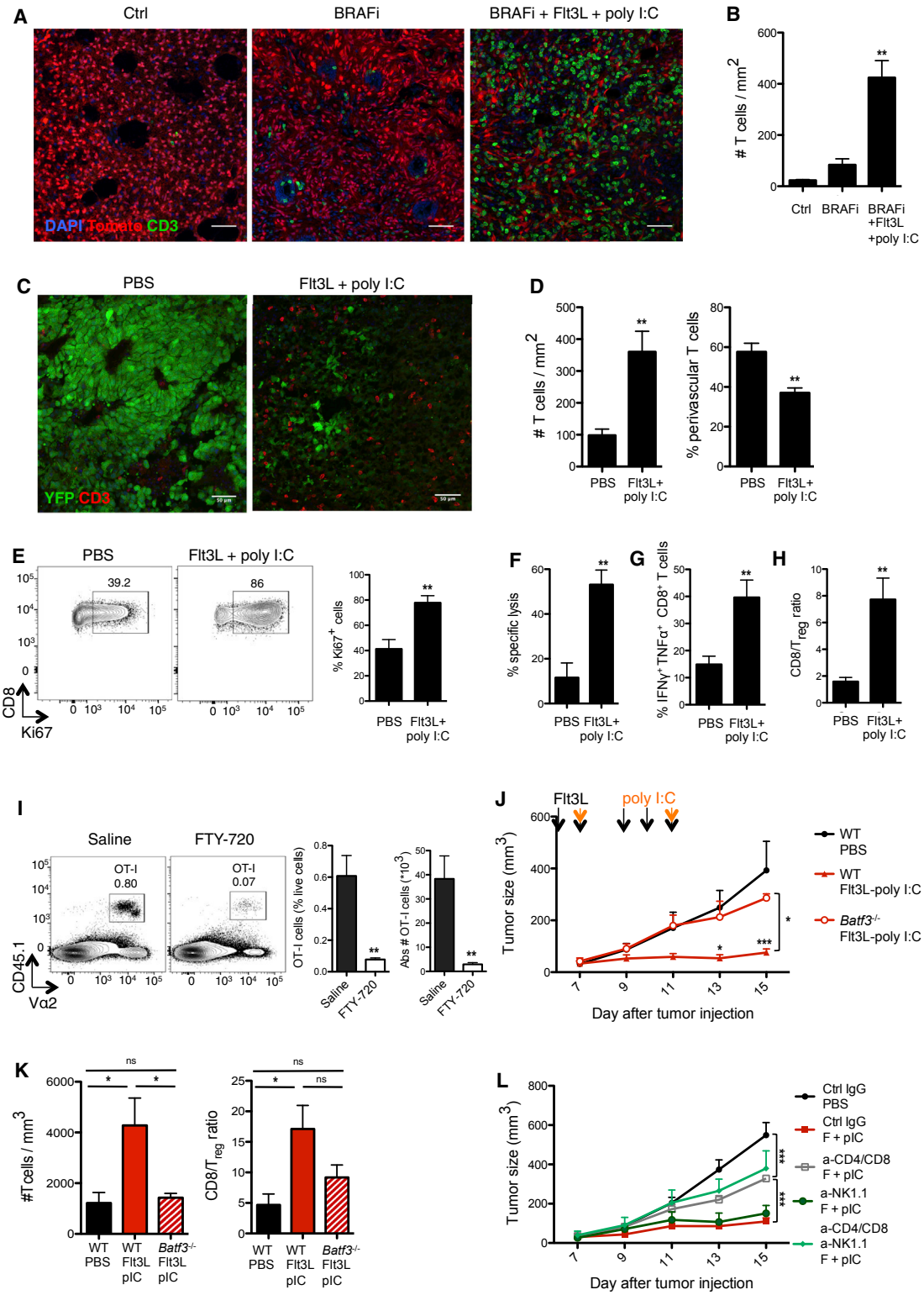

Figure 5. Therapeutic Immunity Induced by FL-pIC Combined Therapy Requires CD103$^+$ DCs and Type I IFN

(A and B) Tomato$^+$ *Braf*-mutant-tumor mice were treated as described in Figure S4B. Two days after the end of treatment, tumors were harvested and frozen.

(A) Representative confocal images of CD3$^+$ T cells (green) infiltrating tumors from the indicated treatment groups.

(B) CD3$^+$ T cell density was quantified from confocal images with Cell Profiler software. Shown is the mean ± SEM of two independent experiments (n = 3 or 4; 12–16 tiled 20× images were analyzed per animal).

(legend continued on next page)

comparison to mice treated with anti-PD-L1 Ab combined with BRAF inhibitors. This was dependent on T cell immunity given that T cell depletion abrogated the clinical benefit of tritherapy on the development of secondary tumors (Figures 6I and 6K).

Altogether, these data show that FL and pIC synergized with PD-L1 blockade to prevent the relapse of *Braf*-mutant melanoma lesions after BRAF inhibition and to protect from tumor rechallenge.

Discussion

In the present study we found that, although most tumor-infiltrating myeloid cells could capture tumor antigens in two mouse melanoma models, tumor-infiltrating CD103$^+$ DCs were uniquely able to transport intact antigens to the TdLN and prime tumor-specific LN CD8$^+$ T cells. CD103$^+$ DCs controlled anti-PD-L1-Ab-mediated anti-tumor immunity; however, PD-L1 inhibition led to modest anti-tumor response, and this response was dramatically increased upon expansion and activation of CD103$^+$ DC at the tumor site.

Our findings that intratumoral CD103$^+$ DCs are uniquely able to transport intact antigens to the TdLN are consistent with the low expression levels of lysosomal degradative enzymes (Miller et al., 2012; Savina et al., 2006) and in line with our previous results showing that lung-resident CD103$^+$ DCs are uniquely able to transport intact viral antigens to the LN upon lung infection with influenza virus (Helft et al., 2012). These results are also in accordance with prior studies showing the requirement for CD103$^+$ DCs in the induction of therapeutic immunity against fibrosarcoma tumor grafts (Hildner et al., 2008).

The low numbers of CD8$^+$ T cells present in B16 and *Braf*-mutant tumors and their limited accumulation upon BRAF and/or PD-L1 blockade might explain the reduced clinical response to these treatments, as previously suggested (Chen and Mellman, 2013; Gajewski et al., 2013). Using an experimental model of breast cancer, recent results revealed that accumulation and activation of intratumoral CD8$^+$ T effector cells is dependent on intratumoral CD103$^+$ DCs (Broz et al., 2014), suggesting that the limited infiltration of CD8$^+$ T cells observed in B16 and *Braf*-mutant lesions could be a consequence of the reduced accumulation of CD103$^+$ DCs in tumors. We have previously reported that tissue resident CD103$^+$ DCs fail to accumulate in injured tissues (Helft et al., 2012), which might explain the limited numbers of CD103$^+$ DCs in tumors. We discovered that FL injections promoted the differentiation of CD103$^+$ DC progenitors already in the bone marrow and their expansion at the tumor site. FL ability to instruct DC progenitors' commitment mainly to the CD103$^+$ DC lineage, although unexpected, is consistent with increased FL receptor expression on CD103$^+$ DCs compared to on CD11b$^+$ DCs (Liu and Nussenzweig, 2010; Miller et al., 2012) and suggests that increased Flt3 signaling might enforce IRF8 signaling, thereby promoting CD103$^+$ DC differentiation.

The expansion of CD103$^+$ DC progenitors was associated with a substantial accumulation at the tumor site of immature CD103$^+$ DCs, which became the predominant myeloid cell population in FL-treated tumors and might explain the increased accumulation of Treg cells in FL-treated tumors and the limited ability of FL to improve tumor response. These results caution the use of FL without a DC maturation agent in patients with tumors. The addition of intratumoral pIC significantly increased tumor-specific CD8$^+$ T cell activation in the TdLN and their accumulation at the tumor site, improving the regression of B16 and *Braf*-mutant tumors. T cells partly controlled the regression of primary tumors and were essential for the reduction of secondary *Braf*-mutant melanoma lesions that developed either spontaneously after the primary tumor or upon tumor rechallenge, suggesting that the tritherapy synergized with BRAF inhibitors to promote a strong and efficient anti-tumor memory T cell immune response that prevented the growth of tumors.

(C and D) B16-YFP-tumor-bearing mice were treated as described in Figure S4A. Two days after the end of treatment, tumors were harvested and frozen.
(C) Shown are representative confocal images of CD3$^+$ T cells (red) infiltrating tumors treated with PBS or FL-pIC.
(D) CD3$^+$ T cell density (left) and proportions of perivascular CD3$^+$ T cells (< 30 μm from CD31$^+$ vessels; right) were quantified from confocal images with Cell Profiler software. Shown is the mean ± SEM of four independent experiments (n = 4–6; 12–16 tiled 20× images were analyzed per animal).
(E–H) B16-tumor-bearing mice were treated as in Figure S4A and tumor-infiltrating T cells were analyzed at day 15, unless specified otherwise.
(E) Representative dot plots (left) and quantification (right) of the frequency of tumor-infiltrating CD8$^+$ T cells expressing the cell-cycle protein Ki67. Graph shows the mean ± SEM of two independent experiments (n = 4).
(F) WT splenocytes were incubated in vitro with ovalbumin$_{257–264}$ peptide and labeled with a high concentration of CFSE (CFSE^{hi}) or incubated with control medium and labeled with low CFSE concentration (CFSE^{low}). The same numbers of CFSE^{hi} and CFSE^{low} splenocytes were coinjected into B16-tumor-bearing mice treated with FL-pIC or PBS at day 16 and analyzed 24 hr later. Shown is the mean ± SEM of one experiment (n = 4 or 5).
(G) CD8$^+$ T cells were analyzed for IFN-γ and TNF-α production after PMA and ionomycin stimulation. Shown is the mean ± SEM of four independent experiments (n = 8).
(H) Tumor-infiltrating CD8$^+$ T cell to Treg cell ratio as the mean ± SEM of four independent experiments (n = 8).
(I) Mice bearing B16-OVA tumors received daily FL injections from day 5 to 9 after tumor challenge; this was followed by one intratumoral injection of pIC at day 9. Two hours after the pIC injection, tumor-bearing mice were injected with 3 × 10^6 naive tumor antigen-specific CD8$^+$ T cells (OT-I) in the presence or absence of the S1P receptor antagonist FTY-720 (from day 9, daily injection as described in the Experimental Procedures). Shown are representative dot plots (left) and quantification of the frequency and absolute numbers of tumor-infiltrating OT-I cells (right) four days after adoptive cell transfer. Graphs show the mean ± SEM of two independent experiments (n = 4 or 5).
(J and K) B16 tumors were injected into WT or *Batf3*$^{-/-}$ mice and treated with FL-pIC. Here, mice received only five injections because CD103$^+$ DCs reappear in *Batf3*$^{-/-}$ mice upon nine FL injections.
(J) Graph shows the mean tumor growth ± SEM of two independent experiments (n = 4–6).
(K) B16 tumors were harvested on day 15. Bar graphs show the intratumoral T cell density as measured by flow cytometry (left) and CD8$^+$ cell to Treg cell ratio (right) in *Batf3*$^{-/-}$ versus WT treated mice. Results are shown as the mean ± SEM of one experiment (n = 4 or 5).
(L) B16-tumor-bearing mice treated with FL-pIC and with anti-CD4, anti-CD8, or anti-NK1.1 Ab or control IgG as described in the Experimental Procedures. Graph shows the mean tumor growth ± SEM of two independent experiments (n = 3–9).
See also Figure S5.

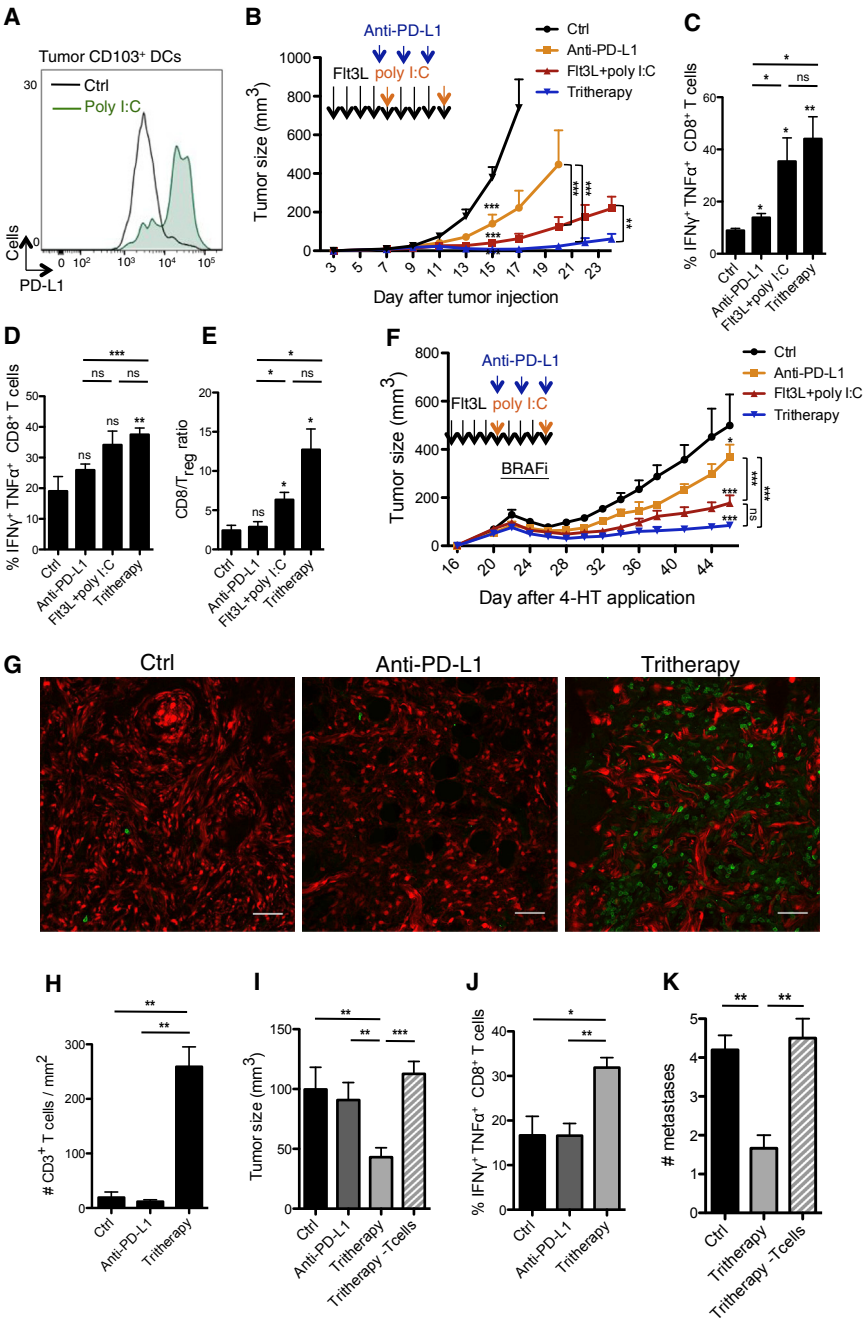

Figure 6. FL and pIC Synergize with anti-PD-L1 Ab Treatment to Enhance Anti-tumor Responses to BRAF Inhibition

(A) B16 tumors were injected with 50 μg pIC or PBS, on days 7 and 11. Histograms show PD-L1 expression on tumor-infiltrating CD103$^+$ DCs, 2 days after the last pIC or PBS injection with one representative example for each group.

(B) B16-tumor-bearing mice were treated with FL-pIC and injected with anti-PD-L1 mAbs or isotype control on days 7, 9, and 11 and assessed for tumor growth. Graph shows the mean tumor growth ± SEM of three independent experiments (n = 5–10).

(C–E) B16-tumor-bearing mice were treated as in (B). On day 15, mice were sacrificed and CD8$^+$ T cells isolated from the TdLN (C) or tumors (D) were analyzed for the production of IFN-γ and TNF-α. Shown is the mean ± SEM of two independent experiments (n = 3–7).

(E) Bar graph shows the intratumoral CD8$^+$ cell to Treg cell ratio as the mean ± SEM of two independent experiments (n = 3–7).

(F) *Braf*-mutant-tumor-bearing mice were treated as indicated by the arrows. In addition to FL-pIC ± anti-PD-L1 Ab therapy (or PBS and rat IgG as a control), all mice were treated with BRAF inhibitors (BRAFi) Admixed Chow for 4 days from day 22 to 26. Graph shows the mean tumor growth ± SEM of two independent experiments (n = 6–12).

(G and H) Tomato$^+$ *Braf*-mutant-tumor-bearing mice were treated with the tritherapy, anti-PD-L1 Ab alone, or PBS/IgG alone and re-challenged 4 weeks later with 4-HT on the other flank, as described in Figure S6A.

(G) Representative confocal images of CD3$^+$ T cells (green) infiltrating the re-challenged tumor.

(H) T cell density quantified by histology with Cell Profiler software. Shown is the mean ± SEM of two independent experiments (n = 3).

(I and J) *Braf*-mutant-tumor and TdLN analyses were performed 4 weeks after the tumor re-challenge, as in (G).

(I) Volume of the re-challenged tumors.

(J) Proportions of CD8$^+$ T in the LN draining the re-challenged tumor producing IFN-γ and TNF-α after PMA-ionomycin stimulation. Shown is the mean ± SEM of two independent experiments (n = 5).

(K) Mice were treated as in Figure S6A, and the number of skin tumors was assessed a month after the end of treatment. Bar graph shows the mean number of skin tumors ± SEM of two independent experiments (n = 5 or 6).

See also Figure S6.

The presence of the human CD103$^+$ DC equivalent, CD141$^+$ DCs, correlates with better outcome in human tumors (Sluijter et al., 2015). Similarly to mouse CD103$^+$ DCs, human CD141$^+$ DCs express IRF8 and high levels of FLT3 and TLR3, and pIC activation of human CD141$^+$ cells leads to the upregulation of PD-L1 (Bogunovic et al., 2011) and to their increased cross-priming of CD8$^+$ T cells (Crozat et al., 2010; Jongbloed et al., 2010; Poulin et al., 2010). This suggests that FL-pIC-anti-PD-L1 Ab tritherapy should help expand and activate tumor-infiltrating DCs and promote the induction of tumor-specific CD8$^+$ T cell immunity in cancer patients.

Compared to monotherapic regimens, the introduction of combination chemotherapy in the 1960s dramatically improved the clinical outcome of numerous tumors (Frei et al., 1958). Our results support the need of novel immunotherapy combination strategies to maximize the induction, expansion, recruitment, and cytotoxic function of tumor-specific CD8$^+$ T cells. We believe that the use of FL to expand CD103$^+$ DC progenitors at the tumor site, followed by intratumoral pIC to induce type I IFN release in the tumor and promote DC immunogenic function, has the potential to transform clinical response to anti-PD-L1 treatment in cancer patients.

EXPERIMENTAL PROCEDURES

Mice

C57BL/6 (CD45.2$^+$) and congenic CD45.1$^+$ C57BL/6 mice were purchased from the Frederick Cancer Research Center or Charles River Laboratories. *Tyr*::*CreER*;*Braf*^{CA}*Pten*^{loxP}*Ctnnb1*^{loxex3} transgenic mice were obtained from Dr. Marcus Bosenberg (Yale University) (Damsky et al., 2011). *Tyr*::*CreER*; *Braf*^{CA}*Pten*^{loxP} mice were purchased from the Jackson Laboratory and crossed to C57BL/6 tdTomato reporter mice (Jackson Laboratory, B6.Cg-Gt (ROSA)26Sor$^{tm14(CAG-tdTomato)Hze}$/J). See Supplemental Experimental Procedures for additional information.

Tumor Induction

The C57BL/6-derived melanoma cell line B16 (Mayordomo et al., 1995), the B16-OVA-transfected clone, and the B16YFP-transfected clone were maintained at 37°C with 5% CO_2 in RPMI medium supplemented with 10% heat-inactivated fetal calf serum, penicillin, and streptomycin (Cellgro). 3×10^5 tumor cells were injected subcutaneously in 50 μl PBS on the flank. *Braf*-mutant melanoma lesions were induced by topical application of 1 μl of 5 mM 4-hydroxytamoxifen. Tumor size was determined by the formula L × W × D where L = length, W = width, and D = depth, on the indicated days.

Treatments

FL (30 μg in 100 μl PBS; Celldex) or control PBS was injected intraperitoneally (i.p.; nine daily injections, unless otherwise noted). High molecular weight pIC (50 μg in 50 μl; InvivoGen) was injected intratumorally. For BRAF inhibition, mice were either fed a chow diet containing 417 mg/kg PLX4720 (Plexxikon) for 4 days or a control diet.

Preparation of Cell Suspensions

Single cell suspension was obtained after tumor digestion with 400 U/ml of type D collagenase (Roche) at 37°C for 1 hr. Hematopoietic cells were enriched by density gradient centrifugation with 40/90 Percoll (GE Healthcare Life Sciences) for 30 min at 2,500 rpm before a 1 min incubation with red blood cell (RBC) lysis buffer (BioLegend) at room temperature. DCs were obtained from LNs after incubation with 400 U/ml Collagenase D (Roche) for 25 min at 37°C. In some cases, DC enrichment was performed with CD11c microbeads according to the manufacturer's instructions (Miltenyi Biotec).

FTY-720 Treatment

FTY-720 was purchased from Sigma, and injected i.p. (200 μl) at a final concentration of 100 μg/ml in saline every day over the indicated time periods.

Re-stimulation and Intracellular Cytokine Staining

Cells were stimulated with 100 ng/ml PMA (Sigma) and 0.5 mg/ml ionomycin (Sigma-Aldrich) at 37°C for 3 hr in the presence of Brefeldin A (10 μg/ml; Sigma) to allow accumulation of intracellular cytokines. After staining of surface markers, cells were fixed and permeabilized, followed by staining of IFN-γ, TNF-α, and Foxp3.

In Vivo Killing Assay

Five days after the last injection of FL and pIC, mice were injected intravenously (i.v.) with spleen cells differentially labeled with 20 or 200 nM CFSE (Invitrogen) and loaded with 10 or 100 nM ovalbumin$_{257–264}$ (referred to as OT-I peptide), respectively. Tumors were collected 24 hr after injection of target cells. Percentage of OVA-specific killing was calculated as described elsewhere (Hermans et al., 2004).

Ab Treatment

Groups of mice were injected with 200 μg anti-CD8 (clone 2.43)-, CD4 (clone GK1.5)-, or NK (clone PK136)- specific mAb (BioXCell) or rat IgG (Sigma) three times at 2-day intervals, starting 2 days before B16 tumor cell injection, followed by a 200 μg dose every 7 days. For PD-L1 blockade, mice were injected i.p. every other day with three doses of 200 μg of anti-PD-L1-specific mAb (10F.9G2, BioXCell) or rat IgG (Sigma).

Statistical Analysis

Graphs were compiled and statistical analyses were performed with Prism software (GraphPad). Statistical significance was evaluated with the unpaired t test when comparing two groups and one-way ANOVA when comparing more than two groups. In all cases, p values < 0.05 were considered statistically significant.

SUPPLEMENTAL INFORMATION

Supplemental Information includes Supplemental Experimental Procedures and six figures and can be found with this article online at http://dx.doi.org/10.1016/j.immuni.2016.03.012.

AUTHOR CONTRIBUTIONS

H.S. and J.I. conceived and performed experiments and wrote the manuscript. A.D., M.L., R.R., M.C-A., M.K, J.A., C.R., B.H., N.T., and S.C. performed experiments. D.H., S.G., N.B., A.K.P., B.B., J.B., and F.G. provided expertise and feedback. M.B. and J.B. provided reagents. A.K.P. provided funding. M.M. conceived experiments, wrote the manuscript, and provided funding.

ACKNOWLEDGMENTS

M.M. was supported by NIH grants R01 CA154947A, R01CA190400, R01 CA173861, U01AI095611, and R01AI104848. H.S. was supported by a postdoctoral fellowship from the Association pour la Recherche contre le Cancer and by the Irvington postdoctoral fellowship of the Cancer Research Institute. D.H. was supported by grants from the Japan Society for the Promotion of Science KAKENHI program (no. 26461438) and the project "The Tenure-Track System Promotion Program" funded by the Ministry of Education, Culture, Sports, Science and Technology. We thank Jill Gregory, manager of academic medical illustration at the Icahn School of Medicine at Mount Sinai, for the graphical abstract. N.B. is co-founder of Checkpoint Sciences and J.B.'s lab receives research funding from Celldex.

Received: May 20, 2015
Revised: November 19, 2015
Accepted: December 21, 2015
Published: April 19, 2016

REFERENCES

Bogunovic, D., O'Neill, D.W., Belitskaya-Levy, I., Vacic, V., Yu, Y.L., Adams, S., Darvishian, F., Berman, R., Shapiro, R., Pavlick, A.C., et al. (2009). Immune profile and mitotic index of metastatic melanoma lesions enhance clinical staging in predicting patient survival. Proc. Natl. Acad. Sci. USA *106*, 20429–20434.

Bogunovic, D., Manches, O., Godefroy, E., Yewdall, A., Gallois, A., Salazar, A.M., Marie, I., Levy, D.E., and Bhardwaj, N. (2011). TLR4 engagement during TLR3-induced proinflammatory signaling in dendritic cells promotes IL-10-mediated suppression of antitumor immunity. Cancer Res. *71*, 5467–5476.

Broz, M.L., Binnewies, M., Boldajipour, B., Nelson, A.E., Pollack, J.L., Erle, D.J., Barczak, A., Rosenblum, M.D., Daud, A., Barber, D.L., et al. (2014). Dissecting the tumor myeloid compartment reveals rare activating antigen-presenting cells critical for T cell immunity. Cancer Cell *26*, 638–652.

Chen, D.S., and Mellman, I. (2013). Oncology meets immunology: the cancer-immunity cycle. Immunity *39*, 1–10.

Cooper, Z.A., Juneja, V.R., Sage, P.T., Frederick, D.T., Piris, A., Mitra, D., Lo, J.A., Hodi, F.S., Freeman, G.J., Bosenberg, M.W., et al. (2014). Response to BRAF inhibition in melanoma is enhanced when combined with immune checkpoint blockade. Cancer Immunol. Res. *2*, 643–654.

Crozat, K., Guiton, R., Contreras, V., Feuillet, V., Dutertre, C.A., Ventre, E., Vu Manh, T.P., Baranek, T., Storset, A.K., Marvel, J., et al. (2010). The XC chemokine receptor 1 is a conserved selective marker of mammalian cells

homologous to mouse CD8alpha+ dendritic cells. J. Exp. Med. *207*, 1283–1292.

Damsky, W.E., Curley, D.P., Santhanakrishnan, M., Rosenbaum, L.E., Platt, J.T., Gould Rothberg, B.E., Taketo, M.M., Dankort, D., Rimm, D.L., McMahon, M., and Bosenberg, M. (2011). β-catenin signaling controls metastasis in Braf-activated Pten-deficient melanomas. Cancer Cell *20*, 741–754.

Fife, B.T., Pauken, K.E., Eagar, T.N., Obu, T., Wu, J., Tang, Q., Azuma, M., Krummel, M.F., and Bluestone, J.A. (2009). Interactions between PD-1 and PD-L1 promote tolerance by blocking the TCR-induced stop signal. Nat. Immunol. *10*, 1185–1192.

Flaherty, K.T., Puzanov, I., Kim, K.B., Ribas, A., McArthur, G.A., Sosman, J.A., O'Dwyer, P.J., Lee, R.J., Grippo, J.F., Nolop, K., and Chapman, P.B. (2010). Inhibition of mutated, activated BRAF in metastatic melanoma. N. Engl. J. Med. *363*, 809–819.

Förster, R., Schubel, A., Breitfeld, D., Kremmer, E., Renner-Müller, I., Wolf, E., and Lipp, M. (1999). CCR7 coordinates the primary immune response by establishing functional microenvironments in secondary lymphoid organs. Cell *99*, 23–33.

Frei, E., 3rd, Holland, J.F., Schneiderman, M.A., Pinkel, D., Selkirk, G., Freireich, E.J., Silver, R.T., Gold, G.L., and Regelson, W. (1958). A comparative study of two regimens of combination chemotherapy in acute leukemia. Blood *13*, 1126–1148.

Fuertes, M.B., Kacha, A.K., Kline, J., Woo, S.R., Kranz, D.M., Murphy, K.M., and Gajewski, T.F. (2011). Host type I IFN signals are required for antitumor CD8+ T cell responses through CD8alpha+ dendritic cells. J. Exp. Med. *208*, 2005–2016.

Gajewski, T.F., Woo, S.R., Zha, Y., Spaapen, R., Zheng, Y., Corrales, L., and Spranger, S. (2013). Cancer immunotherapy strategies based on overcoming barriers within the tumor microenvironment. Curr. Opin. Immunol. *25*, 268–276.

Galon, J., Costes, A., Sanchez-Cabo, F., Kirilovsky, A., Mlecnik, B., Lagorce-Pagès, C., Tosolini, M., Camus, M., Berger, A., Wind, P., et al. (2006). Type, density, and location of immune cells within human colorectal tumors predict clinical outcome. Science *313*, 1960–1964.

Ginhoux, F., Liu, K., Helft, J., Bogunovic, M., Greter, M., Hashimoto, D., Price, J., Yin, N., Bromberg, J., Lira, S.A., et al. (2009). The origin and development of nonlymphoid tissue CD103+ DCs. J. Exp. Med. *206*, 3115–3130.

Guilliams, M., Ginhoux, F., Jakubzick, C., Naik, S.H., Onai, N., Schraml, B.U., Segura, E., Tussiwand, R., and Yona, S. (2014). Dendritic cells, monocytes and macrophages: a unified nomenclature based on ontogeny. Nat. Rev. Immunol. *14*, 571–578.

Hashimoto, D., Miller, J., and Merad, M. (2011). Dendritic cell and macrophage heterogeneity in vivo. Immunity *35*, 323–335.

Helft, J., Manicassamy, B., Guermonprez, P., Hashimoto, D., Silvin, A., Agudo, J., Brown, B.D., Schmolke, M., Miller, J.C., Leboeuf, M., et al. (2012). Cross-presenting CD103+ dendritic cells are protected from influenza virus infection. J. Clin. Invest. *122*, 4037–4047.

Herbst, R.S., Soria, J.C., Kowanetz, M., Fine, G.D., Hamid, O., Gordon, M.S., Sosman, J.A., McDermott, D.F., Powderly, J.D., Gettinger, S.N., et al. (2014). Predictive correlates of response to the anti-PD-L1 antibody MPDL3280A in cancer patients. Nature *515*, 563–567.

Hermans, I.F., Silk, J.D., Yang, J., Palmowski, M.J., Gileadi, U., McCarthy, C., Salio, M., Ronchese, F., and Cerundolo, V. (2004). The VITAL assay: a versatile fluorometric technique for assessing CTL- and NKT-mediated cytotoxicity against multiple targets in vitro and in vivo. J. Immunol. Methods *285*, 25–40.

Hildner, K., Edelson, B.T., Purtha, W.E., Diamond, M., Matsushita, H., Kohyama, M., Calderon, B., Schraml, B.U., Unanue, E.R., Diamond, M.S., et al. (2008). Batf3 deficiency reveals a critical role for CD8alpha+ dendritic cells in cytotoxic T cell immunity. Science *322*, 1097–1100.

Jongbloed, S.L., Kassianos, A.J., McDonald, K.J., Clark, G.J., Ju, X., Angel, C.E., Chen, C.J., Dunbar, P.R., Wadley, R.B., Jeet, V., et al. (2010). Human CD141+ (BDCA-3)+ dendritic cells (DCs) represent a unique myeloid DC subset that cross-presents necrotic cell antigens. J. Exp. Med. *207*, 1247–1260.

Kawai, T., and Akira, S. (2010). The role of pattern-recognition receptors in innate immunity: update on Toll-like receptors. Nat. Immunol. *11*, 373–384.

Keir, M.E., Butte, M.J., Freeman, G.J., and Sharpe, A.H. (2008). PD-1 and its ligands in tolerance and immunity. Annu. Rev. Immunol. *26*, 677–704.

Kroemer, G., Galluzzi, L., Kepp, O., and Zitvogel, L. (2013). Immunogenic cell death in cancer therapy. Annu. Rev. Immunol. *31*, 51–72.

Liu, K., and Nussenzweig, M.C. (2010). Origin and development of dendritic cells. Immunol. Rev. *234*, 45–54.

Longhi, M.P., Trumpfheller, C., Idoyaga, J., Caskey, M., Matos, I., Kluger, C., Salazar, A.M., Colonna, M., and Steinman, R.M. (2009). Dendritic cells require a systemic type I interferon response to mature and induce CD4+ Th1 immunity with poly IC as adjuvant. J. Exp. Med. *206*, 1589–1602.

Matsumoto, M., and Seya, T. (2008). TLR3: interferon induction by double-stranded RNA including poly(I:C). Adv. Drug Deliv. Rev. *60*, 805–812.

Mayordomo, J.I., Zorina, T., Storkus, W.J., Zitvogel, L., Celluzzi, C., Falo, L.D., Melief, C.J., Ildstad, S.T., Kast, W.M., Deleo, A.B., et al. (1995). Bone marrow-derived dendritic cells pulsed with synthetic tumour peptides elicit protective and therapeutic antitumour immunity. Nat. Med. *1*, 1297–1302.

Merad, M., Sathe, P., Helft, J., Miller, J., and Mortha, A. (2013). The dendritic cell lineage: ontogeny and function of dendritic cells and their subsets in the steady state and the inflamed setting. Annu. Rev. Immunol. *31*, 563–604.

Miller, J.C., Brown, B.D., Shay, T., Gautier, E.L., Jojic, V., Cohain, A., Pandey, G., Leboeuf, M., Elpek, K.G., Helft, J., et al.; Immunological Genome Consortium (2012). Deciphering the transcriptional network of the dendritic cell lineage. Nat. Immunol. *13*, 888–899.

Murphy, T.L., Tussiwand, R., and Murphy, K.M. (2013). Specificity through cooperation: BATF-IRF interactions control immune-regulatory networks. Nat. Rev. Immunol. *13*, 499–509.

Page, D.B., Postow, M.A., Callahan, M.K., Allison, J.P., and Wolchok, J.D. (2014). Immune modulation in cancer with antibodies. Annu. Rev. Med. *65*, 185–202.

Poulin, L.F., Salio, M., Griessinger, E., Anjos-Afonso, F., Craciun, L., Chen, J.L., Keller, A.M., Joffre, O., Zelenay, S., Nye, E., et al. (2010). Characterization of human DNGR-1+ BDCA3+ leukocytes as putative equivalents of mouse CD8alpha+ dendritic cells. J. Exp. Med. *207*, 1261–1271.

Salmon, H., Franciszkiewicz, K., Damotte, D., Dieu-Nosjean, M.C., Validire, P., Trautmann, A., Mami-Chouaib, F., and Donnadieu, E. (2012). Matrix architecture defines the preferential localization and migration of T cells into the stroma of human lung tumors. J. Clin. Invest. *122*, 899–910.

Sathe, P., Pooley, J., Vremec, D., Mintern, J., Jin, J.O., Wu, L., Kwak, J.Y., Villadangos, J.A., and Shortman, K. (2011). The acquisition of antigen cross-presentation function by newly formed dendritic cells. J. Immunol. *186*, 5184–5192.

Savina, A., Jancic, C., Hugues, S., Guermonprez, P., Vargas, P., Moura, I.C., Lennon-Duménil, A.M., Seabra, M.C., Raposo, G., and Amigorena, S. (2006). NOX2 controls phagosomal pH to regulate antigen processing during crosspresentation by dendritic cells. Cell *126*, 205–218.

Schlitzer, A., Sivakamasundari, V., Chen, J., Sumatoh, H.R., Schreuder, J., Lum, J., Malleret, B., Zhang, S., Larbi, A., Zolezzi, F., et al. (2015). Identification of cDC1- and cDC2-committed DC progenitors reveals early lineage priming at the common DC progenitor stage in the bone marrow. Nat. Immunol. *16*, 718–728.

Sharma, P., and Allison, J.P. (2015a). The future of immune checkpoint therapy. Science *348*, 56–61.

Sharma, P., and Allison, J.P. (2015b). Immune checkpoint targeting in cancer therapy: toward combination strategies with curative potential. Cell *161*, 205–214.

Sluijter, B.J., van den Hout, M.F., Koster, B.D., van Leeuwen, P.A., Schneiders, F.L., van de Ven, R., Molenkamp, B.G., Vosslamber, S., Verweij, C.L., van den Tol, M.P., et al. (2015). Arming the Melanoma Sentinel Lymph Node through Local Administration of CpG-B and GM-CSF: Recruitment and Activation of

BDCA3/CD141(+) Dendritic Cells and Enhanced Cross-Presentation. Cancer Immunol. Res. *3*, 495–505.

Spranger, S., Koblish, H.K., Horton, B., Scherle, P.A., Newton, R., and Gajewski, T.F. (2014). Mechanism of tumor rejection with doublets of CTLA-4, PD-1/PD-L1, or IDO blockade involves restored IL-2 production and proliferation of CD8(+) T cells directly within the tumor microenvironment. J. Immunother. Cancer *2*, 3.

Spranger, S., Bao, R., and Gajewski, T.F. (2015). Melanoma-intrinsic β-catenin signalling prevents anti-tumour immunity. Nature *523*, 231–235.

Tumeh, P.C., Harview, C.L., Yearley, J.H., Shintaku, I.P., Taylor, E.J., Robert, L., Chmielowski, B., Spasic, M., Henry, G., Ciobanu, V., et al. (2014). PD-1 blockade induces responses by inhibiting adaptive immune resistance. Nature *515*, 568–571.

Yokosuka, T., Takamatsu, M., Kobayashi-Imanishi, W., Hashimoto-Tane, A., Azuma, M., and Saito, T. (2012). Programmed cell death 1 forms negative costimulatory microclusters that directly inhibit T cell receptor signaling by recruiting phosphatase SHP2. J. Exp. Med. *209*, 1201–1217.